Switching of Slow Magnetic Relaxation Dynamics in Mononuclear Dysprosium(III) Compounds with Charge Density

Kwang Soo Lim,[†] José J. Baldoví,[‡] Woo Ram Lee,[†] Jeong Hwa Song,[†] Sung Won Yoon,[§] Byoung Jin Suh,[§] Eugenio Coronado,[‡] Alejandro Gaita-Ariño,*[,‡] and Chang Seop Hong*[,†]

Department of Chemistry, Korea University, Seoul 136-713, Republic of Korea, *Instituto de Ciencia Molecular (ICMol), Universidad de Valencia, C/Catedrático José Beltrán, 2, E-46980 Paterna, Spain and Department of Physics, The Catholic University of Korea, Buchon 420-743, Republic of Korea.*

*To whom correspondence should be addressed. E-mail: alejandro.gaita@uv.es and cshong@korea.ac.kr

Abstract

The symmetry around a Dy ion is recognized to be a crucial parameter dictating magnetization relaxation dynamics. We prepared two similar square-antiprismatic complexes including either two neutral water molecules (**1**) or an anionic nitrate ligand (**2**). We demonstrated that in this case relaxation dynamics is dramatically affected by the introduction of a charged ligand, stabilizing the easy axis of magnetization along the nitrate direction. We also showed that either the application of a dc field or a chemical dilution effectively stops quantum tunneling in the ground state of **2**, thereby increasing the relaxation time by over 3 orders of magnitude at 3.5 K.

Introduction

Because of their weak magnetic exchange coupling, *f*-elements have not been seriously considered as targets for single-molecule magnets (SMMs) until the discovery of slow magnetic relaxation in a series of mononuclear lanthanide compounds with general formula $[Pc_2Ln]^-$ (Pc = phthalocyanide, Ln^{III} = Tb, Dy, Ho).[1-4] The amazing properties of these sandwich complexes, also known as single-ion magnets (SIMs), are mainly determined by the ligand field around the single ion, in contrast to what happens in the classical cluster-type SMMs which are governed by the anisotropic properties of the individual metal ions and their exchange interactions and.[5-7] Since 2008, when the second family of mononuclear SMMs was published,[8] the impact of this class of molecular nanomagnets has dramatically increased, with hundreds of SIMs being reported today.[9-11]

Octacoordinated Dy complexes with square-antiprismatic (SAPR) geometries (D_{4d} symmetry) exhibit relaxation characteristics, and their SMM properties are adjusted by the distortion of local symmetry. In addition, the orientation of the magnetic anisotropy axis can be dominated by small perturbations in the ligand environment, which can also manipulate its dynamic behavior.[14] According to recent research, the magnetic anisotropy of lanthanide ions is strongly affected by electrostatic distribution around the metal center as well as local symmetry.[15-17] Recent studies on SIMs with oblate ions have revealed that, when the electron density of the hard plane was weakened by the attachment of electron-withdrawing groups or by the introduction of a weak-field ligand, magnetic anisotropy increases, resulting in high effective energy barriers.[18-20] A strong magnetic anisotropy was arose from modification of axial ligand fields by negatively charged ligand because the axial negative ligand can stabilization of maximal angular momentum of oblate electron densities. Hence, it is envisioned that electronic properties of the surrounding ligands play a key role in tuning magnetic anisotropy.[26-29] In this regard, theoretical models of a ligand field should always take into account the chemical nature of the ligands around the metal ion. In fact, purely symmetry-based arguments[30] are only applicable to homoleptic complexes. To address this problem, we decided to examine how the introduction of a charged ligand over one of the positions of the coordination sphere controls the slow relaxation dynamics of the SIM. To the best of our knowledge,

this straightforward strategy to characterize the magnetic effect of the ligand charge on a simple monomeric system (not multinuclear compound) has not been previously reported in the literature although it is known that the electron density of the lanthanide ion and the crystal field environment are correlated.

Herein, we designed two compounds—[$Dy(L_{OMe})_2(H_2O)_2$](PF_6) (**1**) and $Dy(L_{OMe})_2(NO_3)$ (**2**)—where Dy ions have identical square-antiprismatic geometries, except that two neutral water molecules coordinate to Dy in **1**, while the negatively charged nitrate ligand coordinates to Dy in **2**. Although the central geometry around Dy in **2** is more distorted than in **1**, SIM characteristics are only evident in **2**. This is contrary to intuitive symmetry considerations, which predict slow magnetic relaxation in those systems having a coordination environment close to square-antiprismatic. In this study, we demonstrate that the mere substitution of one ligand for another with a different effective charge dramatically affects spin energy levels. This notable feature can be mainly ascribed to the dominant charge effect of ligand coordination on the relaxation dynamics over symmetry considerations, switching the SIM behavior on or off.

Experimental Section

Reagent. All chemicals and solvents in the synthesis were reagent grade and used as received. NaL_{OMe} was prepared according to literature procedures.

[$Dy(L_{OMe})_2(H_2O)_2$](PF_6) (1): A mixture of NaL_{OMe} (48.9 mg, 0.10 mmol), NH_4PF_6 (16.3 mg, 0.10 mmol) was dissolved in water (15 mL) and stirred for 10 min. A yellow precipitate was generated as soon as the aqueous solution (2 mL) of $Dy(NO_3)_3{\cdot}5H_2O$ (17.4 mg, 0.05 mmol) was added to the ligand solution. The mixture was stirred at room temperature for 12 h. The precipitate was filtered and washed with water. Yellow crystals formed after vapor diffusion of diethyl ether into a methanol solution of the crude product and were filtered off and dried in air. Yield: 68.4%. Anal. Calcd for $C_{22}H_{50}DyCo_2O_{20}F_6P_7$: C, 21.21; H, 4.05. Found: C, 21.14; H, 4.11.

$[Y(L_{OMe})_2(H_2O)_2](PF_6)$ (1-Y): The Y analogue was obtained by the same procedure as for compound **1**, except that $Y(NO_3)_3{\cdot}6H_2O$ was used instead of Dy(III). Yield: 70.1%. Anal. Calcd for $C_{22}H_{50}YCo_2O_{20}F_6P_7$: C, 22.54; H, 4.30. Found: C, 22.79; H, 4.31.

$[Y_{0.98}Dy_{0.02}(L_{OMe})_2(H_2O)_2](PF_6)$ (diluted-1): An aqueous solution (2 mL) of $Dy(NO_3)_3{\cdot}5H_2O$ (0.001 mmol) and $Y(NO_3)_3{\cdot}6H_2O$ (0.099 mmol) was added to a solution of NaL_{OMe} (0.20 mmol) and NH_4PF_6 (0.20 mmol) in water (15 mL) with stirring. A yellow precipitate was generated and the mixture was stirred at room temperature for 12 h. The precipitate was filtered, washed with water and dried in air. Anal. Calcd for $C_{22}H_{50}Y_{0.98}Dy_{0.02}Co_2O_{20}F_6P_7$: C, 22.51; H, 4.29. Found: C, 22.87; H, 4.29.

$Dy(L_{OMe})_2(NO_3)$ (2): A mixture of NaL_{OMe} (48.9mg, 0.10 mmol) and $Dy(NO_3)_3{\cdot}5H_2O$ (17.4 mg, 0.05 mmol) was dissolved in methanol (1.2 mL). The yellow solution was stirred at room temperature for 4 h and then filtered. Vapor diffusion of diethyl ether into a filtrate afforded yellow crystals. The product was washed with small amount of cold methanol and water. Yield: 58.4%. Anal. Calcd for $C_{22}H_{46}Co_2DyO_{21}P_6N$: C, 23.45; H, 4.11; N, 1.24. Found: C, 23.17; H 4.13; N, 1.19.

$Y(L_{OMe})_2(NO_3)$ (2-Y): The Y analogue was obtained by the same procedure as for compound **2**, except that $Y(NO_3)_3{\cdot}6H_2O$ was used instead of Dy(III). Yield: 49.3%. Anal. Calcd for $C_{22}H_{46}Co_2YO_{21}P_6N$: C, 25.09; H, 4.40; N, 1.33. Found: C, 24.81; H, 4.33; N, 1.21.

$Y_{0.96}Dy_{0.04}(L_{OMe})_2(NO_3)$ (diluted-2): A solution of $Dy(NO_3)_3{\cdot}5H_2O$ (0.002 mmol) and $Y(NO_3)_3{\cdot}6H_2O$ (0.098 mmol) in methanol (0.5 mL) was added to a solution of NaL_{OMe} (0.20 mmol) in methanol (0.7 mL) with stirring. The yellow solution was stirred for 4 h and then diffused with diethyl ether. The yellow powders which had formed were filtered off, washed with cold methanol and water. Anal. Calcd for $C_{22}H_{46}Co_2Y_{0.96}Dy_{0.04}O_{21}P_6N$: C, 25.03; H, 4.39; N, 1.33. Found: C, 24.89; H, 4.30; N, 0.96.

Physical Measurements: Elemental analyses for C, H, and N were performed at the Elemental Analysis Service Center of Sogang University. Infrared spectra were obtained from KBr pellets with a Bomen MB-104 spectrometer. PXRD data were recorded using Cu Kα (λ = 1.5406 Å) on a Rigaku Ultima III diffractometer with a scan speed of 2°/min and a step size of 0.02°. Magnetic susceptibilities for complexes **1** and **2** were carried out using a Quantum Design SQUID

susceptometer (dc) and a PPMS magnetometer (ac). Diamagnetic corrections of all samples were estimated from Pascal's Tables.

Crystallographic Structure Determination X-ray data for **1, 1-Y, 2, 2-Y, diluted-1** and **diluted-2** were collected on a Bruker SMART APEXII diffractometer equipped with graphite monochromated MoKα radiation (λ = 0.71073 Å). Preliminary orientation matrix and cell parameters were determined from three sets of ϕ scans at different starting angles. Data frames were obtained at scan intervals of 0.5° with an exposure time of 10 s per frame. The reflection data were corrected for Lorentz and polarization factors. Absorption corrections were carried out using SADABS. The structures were solved by direct methods and refined by full-matrix least-squares analysis using anisotropic thermal parameters for non-hydrogen atoms with the SHELXTL program. Crystal data for **1, 1-Y, 2, 2-Y, diluted-1** and **diluted-2** are summarized in Table 1.

Results and Discussion

Description of the Structures. To obtain the targeted molecule, we reacted the tripodal ligand $\{CpCo[P(O)(OMe)_2]_3\}^-$, hereafter abbreviated as L_{OMe}^-, with $Dy(NO_3)_3$ in the presence of PF_6^-, which served as the charge balancing anion, to produce **1**. An identical procedure without using PF_6^-, afforded compound **2**. **1** crystallizes in the orthorhombic $P2_12_12$ space group while **2** belongs to the monoclinic system with $P2_1/c$ space group. Each Dy center is octacoordinated by six oxygens from two L_{OMe}^- ligands and two oxygens from two water molecules (**1**) or one nitrate ion (**2**), as shown in Figure 1. From the crystal structures, appreciable differences in Dy-O bond lengths are observed from the binding of the neutral ligands to Dy in **1** and that of the charged ligand to Dy in **2**: The Dy–O bond length ranges from 2.283(1) to 2.488(1) Å in **1** and from 2.289(1) to 2.508(1) Å in **2** (Table S1). To evaluate the exact geometry around the Dy ion, we conducted continuous shape measure analysis.[35] The S_X (X = DD, SAPR; DD = dodecahedron, SAPR = square antiprism) values calculated against ideal symmetry showed that both complexes adopt a distorted SAPR, thereby leading to the local symmetry of Dy^{III} being close to D_{4d} (Table S2). The obtained S_X values indicate that the central geometry around Dy in **1** (S_X = 0.829)

is more ideal to SAPR than that in **2** (S_X = 1.281), as confirmed by the comparison of Figures 1c and 1d. Such an enhanced geometrical distortion in **2** arises from the chelation of NO_3^-. This structural strain is relieved in the coordindation environment around Dy in **1** because two independent water molecules coordinate to Dy instead of one nitrate ion. In the crystal packing of **1**, the cation $[Dy(L_{OMe})_2(H_2O)_2]^+$ is charge-balanced by the insertion of the PF_6^- counter anion. By comparing the structural features of **1** and **2**, one observes that NO_3^- binds to Dy in **2** in a bidentate maner, forming a neutral molecule. The existence of anions in **1** increases the Dy–Dy separation, being the shortest intermolecular Dy–Dy distance 9.318(5) Å and 8.485(5) Å in **1** and **2**, respectively.

Magnetic Properties. The dc magnetic susceptibilities ($\chi_m T$) of **1** and **2** were measured in the temperature range of 2–300 K at 1000 G (Figure 2). The $\chi_m T$ values of **1** and **2** at room temperature are close to the theoretical value of 14.17 cm^3 K mol^{-1} predicted for one Dy^{III} ion ($^6H_{15/2}$, S = 5/2, L = 5, g = 4/3). Upon cooling, the $\chi_m T$ curve first decreases gradually and then decreases more rapidly below 50 K, which is attributed to the thermal depopulation of the Stark sublevels. As shown in the *M* versus *H/T* plot (Figures S1 and S2), below 6 K magnetization linearly increases at low fields, and does not reach saturation even at 7 T and 2.0 K, indicating the possible involvement of magnetic anisotropy arising from Dy. The non-superimposition of *M* curves also confirms the existence of significant magnetic anisotropy as well as low-lying excited levels.

The spin dynamics in **1** was examined by ac magnetic susceptibility measurements under zero dc field and an ac field of 4 G at several oscillating frequencies (*f*) (Figures S3a –S3d). No peaks in the temperature-dependent ac data are present without and with the application of an external field (H_{dc}) of 1000 G. To find the optimal field for blocking of quantum ternneling, we measured the field dependence of ac magnetic susceptibilities for **1** at 2 K (Firure S4). However, any maximum peaks were not observed. In contrast, the dynamic magnetic properties of **2** displayed in Figures 3a and 3b show that, below 8.0 K, the χ_m'' peaks vary with respect to the oscillating frequency despite partly obscured by quantum tunneling, indicating slow magnetic relaxation. The slow spin dynamics in **2** is also corroborated by the frequency-dependent ac data collected at *T* = 2–8 K (Figure S5). As shown in Figure 4, the

curvature in the ln(τ) versus 1/T plot for **2** indicates that spin-lattice relaxation may involve complicated mechanisms such as temperature-independent quantum tunneling (τ_{QTM}), the thermally activated Orbach process ($\propto \exp(-U_{eff}/kT)$), and direct ($\propto T$) and Raman processes ($\propto T^n$). Thus, the relaxation pathways are analyzed by the following equation:

$$\tau^{-1} = \tau_{QTM}^{-1} + AH^2T + CT^n + \tau_0^{-1}exp(-U_{eff}/kT) \qquad (1)$$

The entire data at T = 2–7 K were well fitted with equation 1, giving $\tau_{QTM} = 3.44 \times 10^{-5}$ s, n = 5, C = 0.04547 s^{-1} K^{-5}, $\tau_0 = 2.92 \times 10^{-10}$ s, and an effective energy barrier of U_{eff} = 51.2 cm^{-1} (Figure 4). These results suggest that, in addition to quantum tunneling and Orbach pathways, Raman relaxation is operative in **2**. The Cole–Cole plots at a temperature range of 2–8 K give α parameters of less than 0.28, supporting the narrow distribution of single relaxation processes (Figure S6). To reduce the quantum tunneling effect, we inspected the field-dependent relaxation time and determined the optimal field to be 1.0 kG (Figures S7 and S8). The application of an external field of 1.0 kG to **2** confers prominent slow relaxation (Figures 3c, 3d, S9). The frequency-dependent ac data of **2** under 1.0 kG were collected at T = 2 – 7 K. Both χ_m' and χ_m'' susceptibilities exhibit significant frequency dependence peaks between 4 - 7 K (Figure S10). The pronounced straight line in the Arrhenius plot unveils the complete suppression of the quantum tunneling effect in **2**, thus confirming SIM behavior. The fit of the ac data under 1.0 kG applied dc field to the Arrhenius law was carried out by considering the Raman term (C) in equation 1, resulting in n = 5, C = 0.01071 s^{-1} K^{-5}, $\tau_0 = 3.14 \times 10^{-10}$ s, and U_{eff} = 53.0 cm^{-1}. Thus, the deviated region at a lower temperature is attributed to the Raman relaxation. The α (<0.1) parameter obtained from the Cole–Cole plots is smaller than that for **2** without the applied external field (Figure S11).

It is essential to understand the effect of the magnetic dipolar interaction on quantum tunneling.[38] For this purpose, we treated Y^{3+} instead of Dy^{3+} with NaL_{OMe} under the same experimental conditions: Y-containing products $[Y(L_{OMe})_2(H_2O)_2](PF_6)$ (**1-Y**) and $Y(L_{OMe})_2(NO_3)$ (**2-Y**) were successfully isolated

(Figures S12 and S13). To magnetically dilute the Dy-containing samples, we followed the reaction procedure and partially replaced Dy in **1** (or **2**) with diamagnetic Y^{3+} ions. As shown by the powder X-ray diffraction data in Figures S14 and S15, the profiles of the diluted samples are consistent with the simulated pattern, suggesting that they are isostructural. Elemental and inductively coupled plasma analyses demonstrate that the average ratio of Dy:Y in diluted-**1** and diluted-**2** corresponds to 0.98:0.02 and 0.96:0.04, respectively. The crystal structures of the diluted samples were obtained; the Y–O and (Y,Dy)–O bond lengths range from 2.268(10) to 2.477(12) Å in **1**-**Y**, 2.263(1) to 2.493(1) Å in **2**-**Y**, 2.265(2) to 2.459(3) Å in diluted-**1**, and 2.271(1) to 2.496(1) Å in diluted-**2**, respectively (Figures S16 and S17). Compared with **1** and **2**, the SAPR geometry around the central metal ion in each diluted compound is more distorted, which is due to the inhomogeneity of metal composition (Table S2).

In diluted-**1**, the crystallographic position is occupied by only 2% Dy, with 98% occupation by the diamagnetic Y ion. The neighboring Dy atoms are statistically well separated and thus the dipolar interaction between them can be neglected. However, the peak in χ_m'' was not observed in diluted-**1** even under an external magnetic field (Figures S3e – S3h). While the dipolar coupling is absent for diluted-**2** (Figures 3e, 3f, S18, and S19), in this system, the maximum in χ_m'' varies with frequency, revealing that a slow magnetic relaxation is still clearly visible. This observation implies that the Dy–Dy distance in diluted-**2** is at a sufficient distance such that the dipolar interaction through space is nullified. This leads to the advent of the SIM character in diluted-**2** more distinct than that in **2**. As shown in Figure S20, the narrow distribution ($\alpha < 0.11$) of single relaxation processes is observed from the Cole–Cole plots, and the Arrhenius plot reveals $n = 5$, C = 0.01647 s^{-1} K^{-5}, $\tau_0 = 2.35 \times 10^{-10}$ s, and U_{eff} = 51.5 cm^{-1} (Figure 4). The application of a magnetic field of 1.0 kG affords $n = 5$, C = 0.01098 s^{-1} K^{-5}, $\tau_0 = 2.81 \times 10^{-10}$ s, and U_{eff} = 51.5 cm^{-1}, which are very close to the values without field. This result verifies that the quantum tunneling is sufficiently blocked in the wake of suppressing Dy-Dy dipolar interaction upon dilution. In other words, when **2** is diluted and/or under an applied field, quantum tunneling plays no clear role in

magnetic relaxation; the deviation from linearity can be explained by a Raman process, at least down to the lowest measured frequency of 1 Hz.

From the Arrhenius plots, the energy barrier in diluted-**2** is similar to that in **2** under an external field, suggesting that quantum tunneling can be effectively shut down by applying a magnetic field or minimizing Dy-Dy dipolar interaction. When measuring ac susceptibility for sample **2**, either diluted and/or with an applied magnetic field, at lower frequencies the ac peak moves to lower temperatures. Down to 1 Hz, the linearity in the Arrhenius plot has been gradually lost, indicating the participation of a Raman mechanism, but the systems do not enter the temperature-independent pure tunneling regime. This indicates that by either diluting the sample or by applying a magnetic field, an otherwise very efficient quantum tunneling is being quenched, resulting in a slow magnetic dynamics.

Thus, we show that either the application of a dc field or chemical dilution can effectively stop quantum tunneling in the ground state, thereby increasing the relaxation time notably by over 3 orders of magnitude at a given temperature (3.5 K). Remarkably, these two radically different methods to solve the same problem result in virtually the same final properties, as can be observed by the almost-overlapping data in Figure 4.

Theoretical Calculations. To explain the differences in the magnetic behaviour of both derivatives we have used the REC model[39] introducing the crystal structures of 1 and 2 as input in the SIMPRE computational package. For this purpose, we require two parameters (D_r and Z_i), which describe the ligand-field effects of each type of ligand. In case of the oxygen atoms from the water molecules and the NO_3^- anion, the REC parameters utilized from a recent study,[42] in which a series of polyoxometalate-based lanthanide complexes were modeled, are introduced as starting values. By employing this procedure, an excellent fit of the $\chi_m T$ powder data is obtained with the following parameters for the L_{OMe} ligand (D_r = 0.42 Å and Z_i = 0.84), water oxygen atoms (D_r = 0.78 Å and Z_i = 0.46), and NO_3^- ones (D_r = 0.813 Å and Z_i = 0.31) (Figure 2). This more pronounced effect of the water molecules over the NO_3^- anion reflected by the effective charge is in good agreement with the position of both ligands in the spectrochemical series.

According to our calculations, the difference between the energy levels of both compounds are remarkable (Figure S21), and this explains why slow relaxation of the magnetization is obtained only in **2**. In **2**, the ground-state function is 90% of ±15/2 (g_z = 18.8) and the first excited state is located at approximately 42 cm^{-1}, which is similar to the energy barrier in diluted-**2**. This evidences that the ground state is almost pure and isolated from excited states allowing the observed slow relaxation of the magnetization. Nevertheless, in **1**, we have found a ground state with a wave function described by 69% of ±13/2 and 17% of ±7/2 (g_z = 14.3), with the first excited state located at 1 cm^{-1}, which means that there must be some overlap between the wave functions of both eigenstates. Also, there are some effects that can easily distort the coordination environment: 1) flexibility of water molecules and 2) thermal effects on temperature, i.e., ac measurements are performed at low temperature (between 2 and 10 K) whereas the structures used as input are measured at room temperature (296 K). Thus, we can explain that the presence of two magnetic levels very close in energy, which can even be inverted for the reasons explained above, is compatible with the absence of SIM behavior in **1**.

Meanwhile, in the case of an SAPR coordination mode (D_{4d}), magnetic relaxation tends to depend on the axial compression or elongation of the central geometry. At the same time, quantum tunneling is reported to be associated with the deviation of the twist angle (the rotation of one of the square faces with respect to the C_4 axis). Thus, it appears that the structural distortion from the ideal D_{4d} symmetry facilitates the quantum tunneling of magnetization via transverse anisotropy. In these systems, Kramers doublets are split without the admixture of M_J values. A similar feature has been reported for organometallic SIMs where the local symmetry is regarded as C_s. From the structural aspect, as compared with the Dy coordination of **2**, that of **1** is closer to an ideal SAPR, thereby predicting a larger energy barrier for **2** than **1** with reference to the extent of deviation from perfect local symmetry, as discussed for D_{4d} symmetry. However, this is not the case as SMM properties are only observed for **2** with a more distorted geometry, which implies that symmetry considerations should be counterbalanced by other dominant components. The theoretical analysis of **2** by means of the SIMPRE package and the REC model results in a well-isolated M_J = ±15/2 ground doublet. Although this approach has been used

in the past to calculate the magnetic anisotropy in cases with particularly simple environments,[47] one needs to note the REC model only considers the first coordination sphere and was designed to calculate the spin energy levels and wave functions. In this case, the ligands include a high number of charges beyond the coordination sphere, something that can induce drastic changes in the molecular anisotropy.[14] Thus, it is more adequate to use the MAGELLAN program to determine the magnetic easy axis (Figure 5). This program uses an electrostatic minization strategy using formal charges and takes into account the entire molecule for an inexpensive prediction of the easy axis of magnetization. The application of MAGELLAN to **2** results in a preferred magnetic anisotropy axis which is not parallel to the near-C_4 axis, in sharp contrast with the behaviour observed in square-antiprismatic SIMs. Indeed, the enhancement in the charge density by the nitrate ligand in **2**, as compared with that of the neutral water ligands in **1**, forces the magnetic easy axis to be oriented along the nitrate direction, eventually stabilizing the oblate electron density of the Dy ion. Although it is possible that minor ligand field differences of the ligands or slight differences in coorination geometry can have an effect on the magnetic anisotropy, this finding demonstrates that an efficient approach to generate strong magnetic anisotropy is a direct introduction of a charged ligand to a system of interest.

Conclusions

We have prepared and characterized two Dy^{III} complexes coordinated by neutral water molecules (**1**) or a nitrate anion (**2**), respectively. Notably, in this system, the relaxation dynamics are dominated not by the central symmetry around Dy but by the charge density in the nitrate/water coordinating position. As it is general in science, systematic studies, in which a single parameter is changed, are the way to advance in the rational design of materials with improved properties. In the present example we have shown the key role played by the presence of a charged ligand in a square-antiprismatic Dy complex to tune its magnetic and quantum properties. Furthermore, we have shown that two independent strategies, namely the application of an optimal external field or a magnetic dilution, lead to a suppression of quantum tunneling and thus slows down magnetic relaxation by 3 orders of magnitude.

Author Information

Corresponding Author

*E-mail: alejandro.gaita@uv.es and cshong@korea.ac.kr

Acknowledgment. This work was supported by the Korea CCS R&D Center (KCRC) grant funded by the Korea government (The Ministry of Science, ICT & Future Planning (MSIP)) (NRF-2014M1A8A1049253), by Basic Science Research Program (NRF-2015R1A2A1A10055658), and by Priority Research Centers Program (NRF20120005860). W.R.L. was partly supported by a Korea University grant. We also thank the EU (ERC Advanced Grant SPINMOL and ERC Consolidator Grant DECRESIM), the Spanish MINECO (grant MAT2011-22785), and the Generalitat Valenciana (Prometeo and ISIC Programmes of excellence). A.G.-A. acknowledges funding by the MINECO (Ramón y Cajal contract). J.J.B. thanks the Spanish MINECO for an FPU predoctoral grant.

Supporting Information Available: X-ray crystallographic files in CIF format, additional structural, magnetic data for the complexes. This material is available free of charge via the Internet at http://pubs.acs.org.

References

1. Ishikawa, N.; Sugita, M.; Ishikawa, N.; Koshihara, S.-y.; Kaizu, Y., *J. Phys. Chem. B* **2004,** *108*, 11265-11271.
2. Ishikawa, N.; Sugita, M.; Ishikawa, N.; Koshihara, S.-y.; Kaizu, Y., *J. Am. Chem. Soc.* **2003,** *125*, 8694-8695.
3. Ishikawa, N.; Mizuno, Y.; Takamatsu, S.; Ishikawa, T.; Koshihara, S.-y., *Inorg. Chem.* **2008,** *47*, 10217-10219.
4. Ishikawa, N.; Sugita, M.; Wernsdorfer, W., *J. Am. Chem. Soc.* **2005,** *127*, 3650-3651.
5. Rinehart, J. D.; Fang, M.; Evans, W. J.; Long, J. R., *Nat. Chem.* **2011,** *3*, 538-542.
6. Rinehart, J. D.; Fang, M.; Evans, W. J.; Long, J. R., *J. Am. Chem. Soc.* **2011,** *133*, 14236-14239.
7. Demir, S.; Jeon, I.-R.; Long, J. R.; Harris, T. D., *Coord. Chem. Rev.* **2015,** *289-290*, 149-176.
8. AlDamen, M. A.; Clemente-Juan, J. M.; Coronado, E.; Martí-Gastaldo, C.; Gaita-Arinõ, A., *J. Am. Chem. Soc.* **2008,** *130*, 8874-8875.
9. Woodruff, D. N.; Winpenny, R. E.; Layfield, R. A., *Chem. Rev.* **2013,** *113*, 5110-5148.
10. Sorace, L.; Benelli, C.; Gatteschi, D., *Chem. Soc. Rev.* **2011,** *40*, 3092-3104.

11. Jia, L.; Chen, Q.; Meng, Y.-S.; Sun, H.-L.; Gao, S., *Chem. Commun.* **2014,** *50*, 6052-6055.

12. Yin, D.-D.; Chen, Q.; Meng, Y.-S.; Sun, H.-L.; Zhang, Y.-Q.; Gao, S., *Chem. Sci.* **2015,** *6*, 3095-3101.

13. Shang, H.; Zeng, S.; Wang, H.; Dou, J.; Jiang, J., *Sci. Rep.* **2015,** *5*, 8838.

14. Cucinotta, G.; Perfetti, M.; Luzon, J.; Etienne, M.; Car, P. E.; Caneschi, A.; Calvez, G.; Bernot, K.; Sessoli, R., *Angew. Chem. Int. Ed.* **2012,** *51*, 1606-1610.

15. Aravena, D.; Ruiz, E., *Inorg. Chem.* **2013,** *52*, 13770-13778.

16. Chilton, N. F.; Collison, D.; McInnes, E. J.; Winpenny, R. E.; Soncini, A., *Nat. Commun.* **2013,** *4*, 2551-2557.

17. Ungur, L.; Le Roy, J. J.; Korobkov, I.; Murugesu, M.; Chibotaru, L. F., *Angew. Chem. Int. Ed.* **2014,** *53*, 4413-4417.

18. Tuna, F.; Smith, C. A.; Bodensteiner, M.; Ungur, L.; Chibotaru, L. F.; McInnes, E. J.; Winpenny, R. E.; Collison, D.; Layfield, R. A., *Angew. Chem. Int. Ed.* **2012,** *51*, 6976-6980.

19. Demir, S.; Zadrozny, J. M.; Long, J. R., *Chem. Eur. J.* **2014,** *20*, 9524-9529.

20. Habib, F.; Brunet, G.; Vieru, V.; Korobkov, I.; Chibotaru, L. F.; Murugesu, M., *J. Am. Chem. Soc.* **2013,** *135*, 13242-13245.

21. Chilton, N. F.; Goodwin, C. A. P.; Mills, D. P.; Winpenny, R. E. P., *Chem. Commun.* **2015,** *51*, 101-103.

22. Chilton, N. F., *Inorg. Chem.* **2015,** *54*, 2097-2099.

23. Rinehart, J. D.; Long, J. R., *Chem. Sci.* **2011,** *2*, 2078-2085.

24. Gregson, M.; Chilton, N. F.; Ariciu, A.-M.; Tuna, F.; Crowe, I. F.; Lewis, W.; Blake, A. J.; Collison, D.; McInnes, E. J. L.; Winpenny, R. E. P.; Liddle, S. T., *Chem. Sci.* **2016,** *7*, 155-165.

25. Li, X. L.; Li, H.; Chen, D. M.; Wang, C.; Wu, J.; Tang, J.; Shi, W.; Cheng, P., *Dalton Trans.* **2015,** *44*, 20316-20320.

26. Sun, W.-B.; Yan, P.-F.; Jiang, S.-D.; Wang, B.-W.; Zhang, Y.-Q.; Li, H.-F.; Chen, P.; Wang, Z.-M.; Gao, S., *Chem. Sci.* **2016,** *7*, 684-691.

27. Pugh, T.; Tuna, F.; Ungur, L.; Collison, D.; McInnes, E. J.; Chibotaru, L. F.; Layfield, R. A., *Nat. Commun.* **2015,** *6*, 7492.

28. Brunet, G.; Habib, F.; Korobkov, I.; Murugesu, M., *Inorg. Chem.* **2015,** *54*, 6195-6202.

29. Cao, W.; Gao, C.; Zhang, Y.-Q.; Qi, D.; Liu, T.; Wang, K.; Duan, C.; Gao, S.; Jiang, J., *Chem. Sci.* **2015,** *6*, 5947-5954.

30. Baldovi, J. J.; Cardona-Serra, S.; Clemente-Juan, J. M.; Coronado, E.; Gaita-Arino, A.; Palii, A., *Inorg. Chem.* **2012,** *51*, 12565-12574.

31. Coutinho, J. T.; Antunes, M. A.; Pereira, L. C. J.; Marçalo, J.; Almeida, M., *Chem. Commun.* **2014,** *50*, 10262-10264.

32. Lin, S. Y.; Guo, Y. N.; Guo, Y.; Zhao, L.; Zhang, P.; Ke, H.; Tang, J., *Chem. Commun.* **2012,** *48*, 6924-6926.

33. Klaui, W.; Eberspach, W.; Gütlich, P., *Inorg. Chem.* **1987,** *26*, 3977-3982.

34. Klaui, W.; Eberspach, W.; Schwarz, R., *J. Organomet. Chem.* **1983,** *252*, 347-357.

35. Alvarez, S.; Alemany, P.; Casanova, D.; Cirera, J.; Llunell, M.; Avnir, D., *Coord. Chem. Rev.* **2005,** *249*, 1693-1708.

36. Brown, A. J.; Pinkowicz, D.; Saber, M. R.; Dunbar, K. R., *Angew. Chem. Int. Ed.* **2015,** *54*, 5864-5868.

37. Meihaus, K. R.; Minasian, S. G.; Lukens, W. W., Jr.; Kozimor, S. A.; Shuh, D. K.; Tyliszczak, T.; Long, J. R., *J. Am. Chem. Soc.* **2014,** *136*, 6056-6068.

38. Habib, F.; Lin, P. H.; Long, J.; Korobkov, I.; Wernsdorfer, W.; Murugesu, M., *J. Am. Chem. Soc.* **2011,** *133*, 8830-8833.

39. Baldovi, J. J.; Borras-Almenar, J. J.; Clemente-Juan, J. M.; Coronado, E.; Gaita-Arino, A., *Dalton Trans.* **2012,** *41*, 13705-13710.

40. Baldovi, J. J.; Cardona-Serra, S.; Clemente-Juan, J. M.; Coronado, E.; Gaita-Arino, A.; Palii, A., *J. Comput. Chem.* **2013,** *34*, 1961-1967.

41. Baldoví, J. J.; Clemente-Juan, J. M.; Coronado, E.; Gaita-Ariño, A.; Palii, A., *J. Comput. Chem.* **2014,** *35*, 1930-1934.

42. Baldoví, J. J.; Clemente-Juan, J. M.; Coronado, E.; Duan, Y.; Gaita-Ariño, A.; Giménez-Saiz, C., *Inorg. Chem.* **2014,** *53*, 9976-9980.

43. Wang, H.; Wang, K.; Tao, J.; Jiang, J., *Chem. Commun.* **2012,** *48*, 2973-2975.

44. Bi, Y.; Guo, Y.-N.; Zhao, L.; Guo, Y.; Lin, S.-Y.; Jiang, S.-D.; Tang, J.; Wang, B.-W.; Gao, S., *Chem. Eur. J.* **2011,** *17*, 12476-12481.

45. Jeletic, M.; Lin, P.-H.; Roy, J. J. L.; Korobkov, I.; Gorelsky, S. I.; Murugesu, M., *J. Am. Chem. Soc.* **2011,** *133*, 19286-19289.

46. Jiang, S.-D.; Wang, B.-W.; Sun, H.-L.; Wang, Z.-M.; Gao, S., *J. Am. Chem. Soc.* **2011,** *133*, 4730-4733.

47. Baldoví, J. J.; Clemente-Juan, J. M.; Coronado, E.; Gaita-Ariño, A., *Inorg. Chem.* **2014,** *53*, 11323-11327.

Table 1. . Crystallographic Data for 1, 1-Y, 2, 2-Y, diluted-1 and diluted-2.

$^{a}R1=\Sigma||F_O|-|F_C||/\Sigma|F_C|$, $^{b}wR2 = [\Sigma w(F_O^2 - F_C^2)^2/\Sigma w(F_O^2)^2]^{1/2}$

	1	1-Y	diluted-1	2	2-Y
formula	$C_{22}H_{50}Co_2DyF_6O_{20}P_7$	$C_{22}H_{50}Co_2YF_6O_{20}P_7$	$C_{22}H_{50}Co_2Y_{0.98}Dy_{0.02}F_6O_{20}P_7$	$C_{22}H_{46}Co_2DyNO_{21}P_6$	$C_{22}H_{46}Co_2YNO_{21}P_6$
Mr	1245.77	1172.18	1173.65	1126.78	1053.19
T (K)	296(2)	296(2)	296(2)	296(2)	296(2)
crystal system	orthorhombic	orthorhombic	orthorhombic	monoclinic	monoclinic
space group	P2(1)2(1)2	P2(1)2(1)2	P2(1)2(1)2	P2(1)/c	P2(1)/c
a (Å)	11.0948(6)	11.027(8)	11.036(2)	12.3285(7)	12.286(5)
b (Å)	21.2245(12)	21.187(11)	21.151(4)	19.4664(10)	19.4333(8)
c (Å)	9.3176(5)	9.303(7)	9.2922(15)	16.7740(10)	16.7538(6)
α (°)	90	90	90	90	90
β (°)	90	90	90	102.686(3)	102.943(3)
γ (°)	90	90	90	90	90
V (Å^3)	2194.1(2)	2173(2)	2169(7)	3927.4(4)	3898.5(3)
Z	2	2	2	4	4
ρ_{calc} (g cm^{-3})	1.886	1.791	1.797	1.906	1.794
μ (mm^{-1})	2.783	2.432	2.445	3.042	2.643
F(000)	1242	1188	1189	2252	2144
total reflections	10238	7753	12960	62195	65387
GOF	1.060.	0.935	0.951	1.061	0.940
R1[a] (I≥2σ(I))	0.0488	0.0825	0.0558	0.0495	0.0693
wR2[b] (I≥2σ(I))	0.1335	0.1453	0.1061	0.1084	0.1299

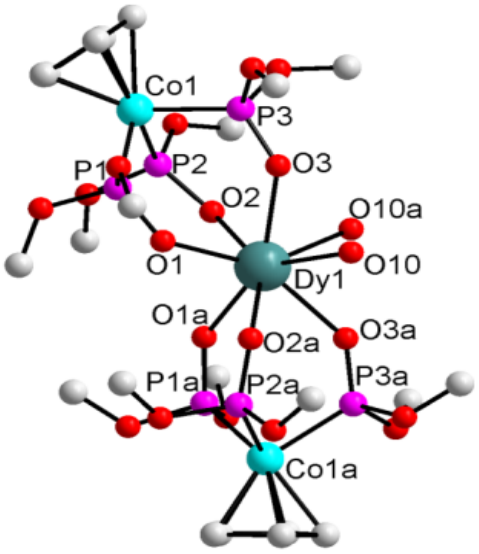

(a)

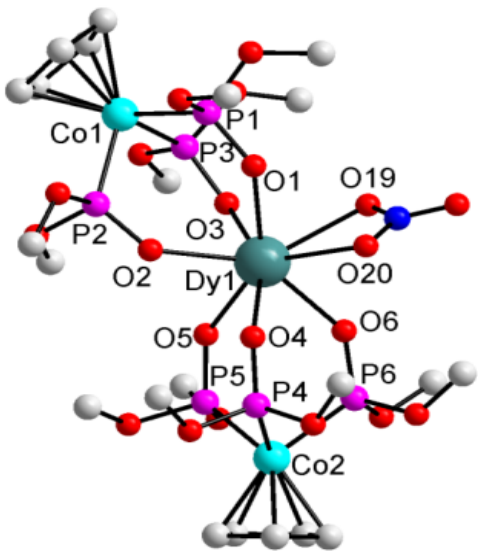

(b)

(c) **(d)**

Figure 1. (a) Molecular structure of the cationic part of **1**. Symmetry code: a = 1-x, -y, z. (b) Molecular view of **2** (c) The D_{4d} local symmetry of **1**. (d) The D_{4d} coordination environment of **2**.

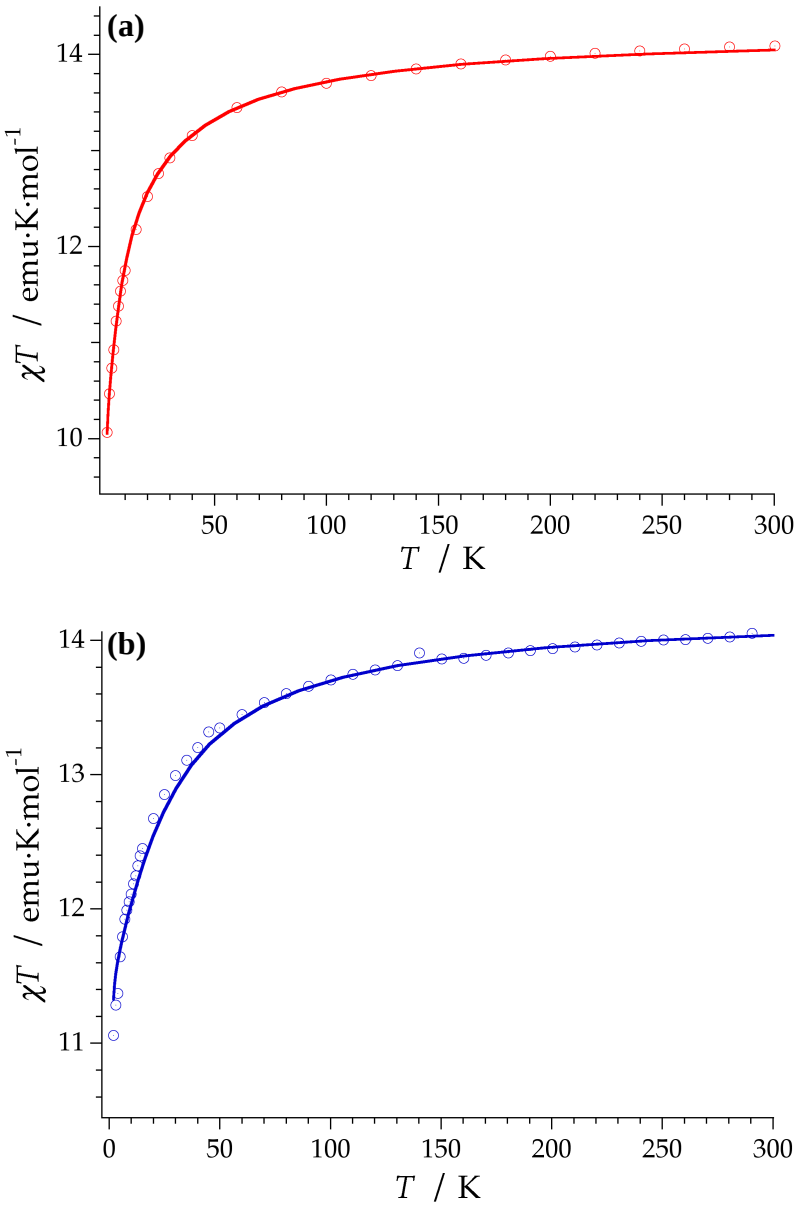

Figure 2. Fitting of the experimental χT products of **1** (a) and **2** (b) from 2 to 300 K using the REC model in the SIMPRE package (solid line).

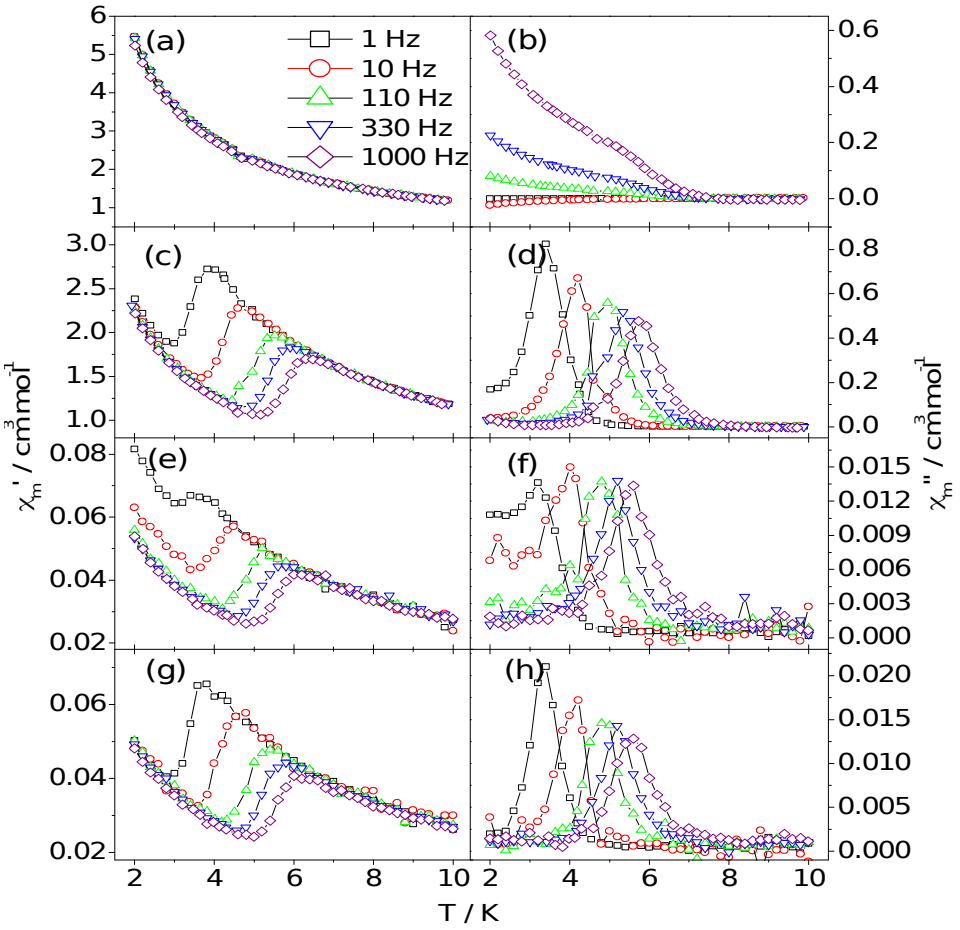

Figure 3. Temperature dependence of in-phase (χ_m') and out-of-phase (χ_m'') ac susceptibility at H_{dc} = 0 (a, b) and 1.0 kG (c, d) for **2**, and at H_{dc} = 0 (e, f) and 1.0 kG (g, h) for diluted-**2**.

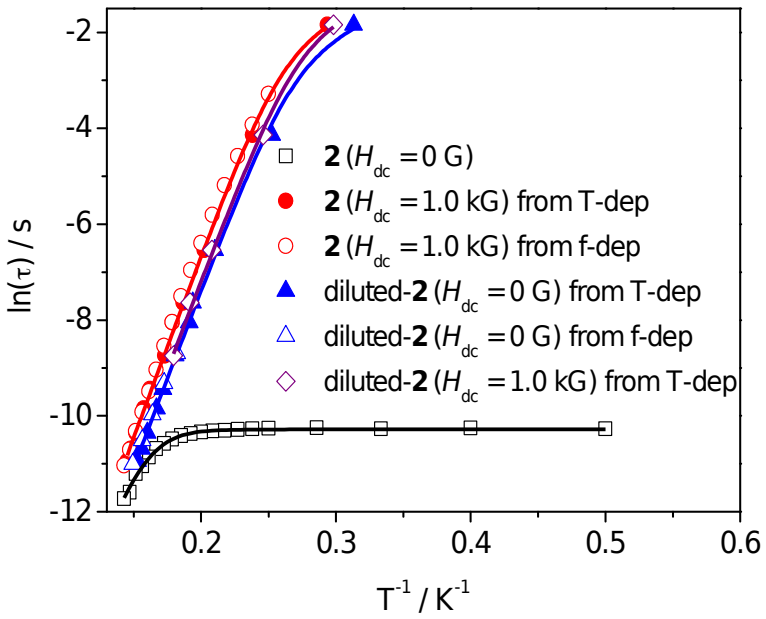

Figure 4. Arrhenius plots of relaxation time data for **2** and diluted-**2**.

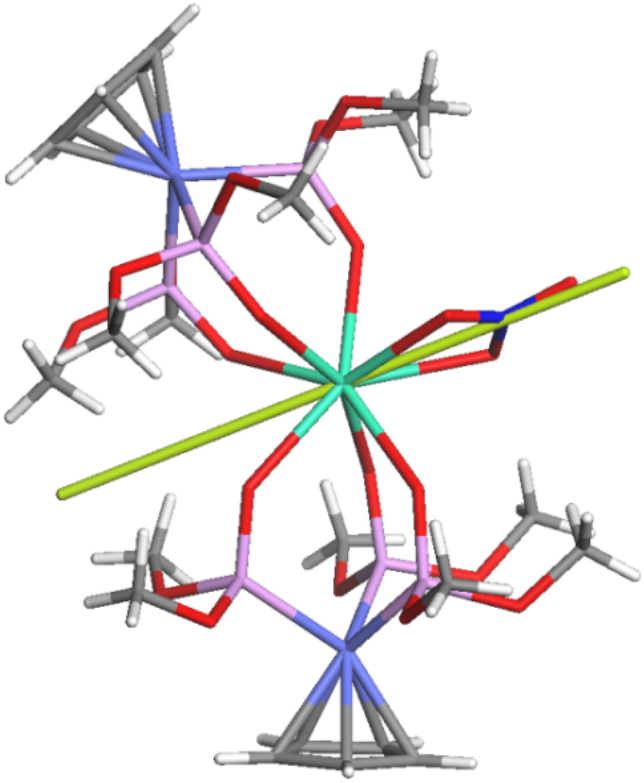

Figure 5. Orientation of the anisotropy axis of **2**.

Table of Contents

Switching of Slow Magnetic Relaxation Dynamics in Mononuclear Dysprosium(III) Compounds with Charge Density

K.S. Lim, J.J. Baldoví, W.R. Lee, J. H. Song, S. W. Yoon, B. J. Suh, E. Coronado, A. Gaita-Ariño* and C.S. Hong*

Two square-antiprismatic complexes containing either two neutral water molecules or an anionic nitrate ligand were prepared. Relaxation dynamics were dramatically affected by the introduction of a charged ligand and the application of either a dc field or chemical dilution.